Letter

Synthetic U(1) gauge invariance in a spin-1 Bose gas

Chunping Gao, ¹ Jinghu Liu, ¹ Maolin Chang, ¹ Han Pu ⁰, ², * and Li Chen ⁰, [†]

¹Institute of Theoretical Physics and State Key Laboratory of Quantum Optics and Quantum Optics Devices,

Shanxi University, Taiyuan 030006, China

²Department of Physics and Astronomy, and Rice Center for Quantum Materials, Rice University, Houston, Texas 77005, USA



(Received 2 April 2022; revised 3 September 2022; accepted 12 October 2022; published 1 November 2022)

Recent experimental realizations of the U(1) gauge invariance [Nature (London) 587, 392 (2020); Science 367, 1128 (2020)] open a door for quantum simulation of elementary particles and their interactions using ultracold atoms. Stimulated by such exciting progress, we propose a platform—a spin-1 Bose-Einstein condensate—to simulate the deconfined lattice Schwinger model. Unlike previous platforms, it is shown that the atomic interactions in the spin-1 condensate naturally lead to a matter-field interaction term which respects the U(1) gauge symmetry. As a result, a new \mathbb{Z}_3 -ordered phase with threefold ground-state degeneracy emerges in the phase diagram. The \mathbb{Z}_3 phase connects to the disordered phase by a three-state Potts criticality, which is in contrast to the conventional Coleman's transition with Ising criticality. Furthermore, the ordered state is constructed by a set of weak quantum scars, which is responsible for the anomalously slow dynamics as it is quenched to a special point in the phase diagram. Our proposal provides a platform for extracting emergent physics in synthetic gauge systems with matter-field interactions.

DOI: 10.1103/PhysRevResearch.4.L042018

I. INTRODUCTION

Gauge invariance, which refers to the coordinated dynamics of matter and gauge fields being restricted by local symmetries at each spacetime location [1], has fundamentally shaped our understanding of interacting elementary particles in quantum electrodynamics (QED) [2] and quantum chromodynamics [3-5]. While a number of breakthroughs in synthesizing gauge fields in cold atoms have been made over the last decade [6], including the experimental realization of artificial electric [7] and magnetic fields [8], spin-orbit coupling [9–11], and the density-dependent gauge field [12,13], none of them is essentially endowed with local symmetry. Very recently, this situation has been changed by two cold-atom groups [14,15] who experimentally realized the deconfined lattice Schwinger model (LSM) with topological angle being equal to π [16]. As a result, counterparts of physical phenomena in the traditional LSM, such as the Coleman's phase transition [16], string inversion, and meson formation [17,18], are expected to be observed. It has been also shown recently that a Rydberg chain with nearest-site Rydberg blockade [19] can also be mapped to a deconfined LSM [20] with U(1) gauge invariance.

Motivated by the recent experimental progress, we propose a platform to simulate the deconfined LSM by loading spin-1

Published by the American Physical Society under the terms of the Creative Commons Attribution 4.0 International license. Further distribution of this work must maintain attribution to the author(s) and the published article's title, journal citation, and DOI.

bosonic atoms (with three spin modes $\hat{b}_{\sigma=\{\pm 1,0\}}$) in an optical lattice. Our basic idea can be summarized as follows [see Fig. 1(a)]: at each site, the matter field is realized by b_{+1} modes, whereas the gauge field is realized by the mode \hat{b}_0 ; the matter-gauge interaction arises from the spin-exchange interaction between \hat{b}_0 and $\hat{b}_{\pm 1}$; an additional Raman process is employed connecting independent sites into a chain. Remarkably, our effective Hamiltonian carries a four-fermion (matter-field) interaction term that has no counterpart in the conventional LSM [14–18]. This term gives rise to several new physics in both ground-state and quench dynamics. In the equilibrium phase diagram, this term leads to a \mathbb{Z}_3 -ordered phase which connects to the disordered phase D and the \mathbb{Z}_2 -ordered phase by a second-order Potts criticality and a first-order transition, respectively. This is in sharp contrast to the conventional LSM without matter-field interaction, where only an Ising-type transition $D-\mathbb{Z}_2$ can be observed. This $D\text{-}\mathbb{Z}_2$ transition is also known as the Coleman's transition in some literature [21,22]. Additionally, we find that the Potts criticality is intimately related to the anomalous quench dynamics, and the quantum scars associated with the \mathbb{Z}_3 state thus is of help in tracing the origin of \mathbb{Z}_3 -related quantum

Although models with four-fermion interactions $(\bar{\psi}\psi)^2$ are fundamental in quantum field theory [23,24], such as the Gross-Neveu model [25] and the Thirring model [26], there have been few studies on the synthetic gauge fields in these models. Since our effective model naturally contains a matter-field (fermion) interaction, our proposal thus paves the way for the study of strongly correlated Dirac fermion with gauge invariance. We note that the experimental setup in Ref. [14] cannot support a strong matter-field interaction, since there, the matter-field interaction corresponds to the next-neighboring-site interaction, which is generally much

^{*}hpu@rice.edu

[†]lchen@sxu.edu.cn

weaker than the on-site and nearest-neighboring interactions. On the other hand, the lattice sites in experiment Ref. [15] have not been linked to form a chain; thus no matter-field interaction exists. Furthermore, their setup involves two species of spin-1/2 atoms, whose interaction are more difficult to control than the single-species spin-1 system [27,28] proposed in our scheme.

II. MODEL

The U(1) LSM is represented by the following Hamiltonian [14,15,17,18,20]:

$$\hat{H}_{LSM} = -t \sum_{j} (\hat{\psi}_{j-1}^{\dagger} \hat{U}_{j-1,j} \hat{\psi}_{j} + \text{H.c.})$$

$$+ m \sum_{j} (-1)^{j} \hat{\psi}_{j}^{\dagger} \hat{\psi}_{j} + \frac{1}{2} \sum_{j} \hat{E}_{j-1,j}^{2}, \qquad (1)$$

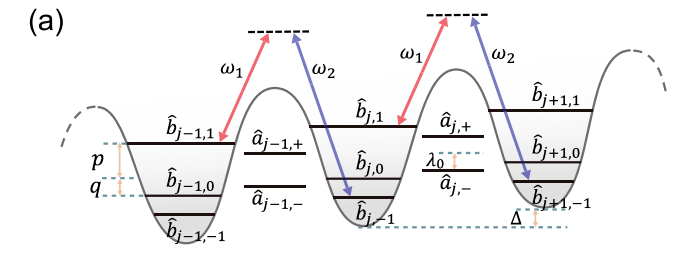
where $\hat{\psi}_j$ is the fermionic matter field at site j, $\hat{U}_{j-1,j}$ and $\hat{E}_{j-1,j}$ account for the gauge degree of freedom living on the link (j-1,j), respectively denoting the transporter and the electric field, and satisfying the $\mathfrak{su}(2)$ algebra $[\hat{E}_{j-1,j},\hat{U}_{k-1,k}] = \delta_{j,k}\hat{U}_{k-1,k}$. The first term of \hat{H}_{LSM} indicates the matter-gauge interaction, the second term denotes the staggered mass in odd and even sites, and the last term accounts for the electric energy. In experiments [14,15], the gauge fields were realized by spin-1/2 Pauli spins, i.e., $\hat{U}_{j-1,j} = \hat{\sigma}_{j-1,j}^+$ and $\hat{E}_{j-1,j} = \hat{\sigma}_{j-1,j}^z/2$, and the resulting model is also called the quantum link model [29]. In this case the electric energy is just a constant since $\hat{E}_{j-1,j}^2 = 1/4$, which can be neglected. The realized quantum link model corresponds to the deconfined LSM in the continuous limit with topological angle fixed to π [20,21].

We simulate the deconfined LSM model by loading a spin-1 Bose gas deeply in a one-dimensional optical lattice along the x direction, as is schematically shown in Fig. 1(a). Under the tight-binding approximation, the lowest-band Wannier mode of the site j is denoted by $\hat{b}_{j,\sigma}$ with bare spin $\sigma = \{1, 0, -1\}$. We introduce a biased magnetic field and a gradient potential, where the former splits the Zeeman levels with the linear and quadratic splittings respectively denoted by p and q, and the latter provides a spin-independent tilt with strength Δ [30,31]. To connect different sites into a chain we adopt the well-established technique of Raman-assisted hopping [32], as is shown in Fig. 1(a). The Λ -type Raman transition can be realized by the combined effects of the lattice beam (along x direction with frequency ω_1) and an additional traveling wave (along z direction with frequency ω_2). Now we write out the total Hamiltonian in the laboratory frame as (setting $\hbar = 1$)

$$\hat{H} = \hat{H}_0 + \hat{H}_{\text{int}},\tag{2}$$

with \hat{H}_0 the single-particle Hamiltonian given by

$$\begin{split} \hat{H}_0 &= \sum_j \left[p \hat{F}_j^z + q \hat{\Xi}_j + j \Delta \hat{n}_j \right. \\ &+ \lambda_0 (e^{-i\delta\omega t} \hat{b}_{j,1}^\dagger \hat{b}_{j+1,-1} + \text{H.c.}) \right], \end{split} \tag{3}$$



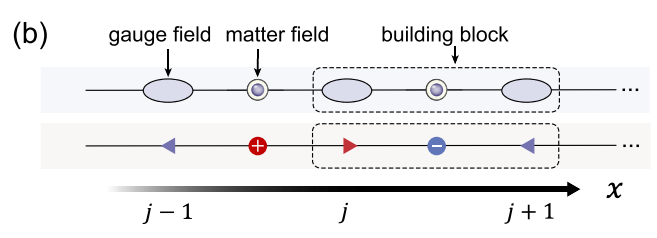


FIG. 1. (a) Schematic of our model in the laboratory frame. p and q respectively denote the linear and quadratic Zeeman splittings, and Δ is a gradient potential. ω_1 and ω_2 are the frequencies of the lattice beam along x direction and the traveling wave along z direction. The two beams resonantly couple the modes $\hat{b}_{j,1}$ and $\hat{b}_{j+1,-1}$, forming a Λ -type Raman process. (b) Upper panel: diagram of the U(1) lattice gauge model, where the gauge and the matter fields correspond to the bare mode $\hat{b}_{j,0}$ and the dressed mode $\hat{a}_{j,-}$ in subfigure (a), respectively. Lower panel: QED analog composed by electrons and positrons (matter fields), and electric fields (gauge fields). A building block surrounded by the dashed line consists of two neighboring gauge fields and one matter field in the middle.

and \hat{H}_{int} the interaction Hamiltonian [33,34] given by

$$\hat{H}_{\text{int}} = \frac{U_0}{2} \sum_{j} \hat{n}_j (\hat{n}_j - 1) + \frac{U_2}{2} \sum_{j} (\hat{\mathbf{F}}_j^2 - 2\hat{n}_j). \tag{4}$$

Here, $\hat{F}_{j}^{\mu} \equiv \sum_{\sigma,\sigma'} \hat{b}_{j,\sigma}^{\dagger} S_{\sigma\sigma'}^{\mu} \hat{b}_{j,\sigma'}$ are the local spin operators with $S^{\mu=x,y,z}$ the generalized spin-1 Pauli matrices, and $\hat{n}_{j} = \sum_{\sigma} \hat{n}_{j,\sigma}$ is the local number operator with $\hat{n}_{j,\sigma} = \hat{b}_{j,\sigma}^{\dagger} \hat{b}_{j,\sigma}$, and $\hat{\Xi}_{j} = \hat{n}_{j,1} + \hat{n}_{j,-1}$. U_{0} and U_{2} in $\hat{H}_{\rm int}$ indicate the strengths of the spin-independent and the spin-dependent interaction, respectively. The last term in \hat{H}_{0} characterizes the Raman coupling, with $\delta\omega = \omega_{2} - \omega_{1}$ the frequency difference between the two Raman beams and λ_{0} the strength of Raman coupling.

We obtain the time-independent Hamiltonian in the rotating frame, i.e., $\hat{H}_0 \rightarrow \hat{U}(t)\hat{H}_0\hat{U}^{\dagger}(t) - i\hat{U}(t)\partial_t\hat{U}^{\dagger}(t)$, where

$$\hat{U}(t) = \prod_{j} \exp\left[i(j\Delta t)\hat{n}_{j} + i\left(\frac{\delta\omega t}{2} + \frac{\Delta t}{2}\right)\hat{F}_{j}^{z}\right]$$
 (5)

is a unitary transformation to eliminate both the phase factor $e^{i\delta\omega t}$ in the hopping term and the gradient term [32,35,36]. In such a frame, we have

$$\hat{H}_0 = \sum_{j} \left[p' \hat{F}_j^z + q \hat{\Xi}_j + \lambda_0 (\hat{b}_{j,1}^{\dagger} \hat{b}_{j+1,-1} + \text{H.c.}) \right], \quad (6)$$

with $p'=p-\Delta/2-\delta\omega/2$. We will focus on the case under Raman resonance, i.e., p'=0. The resonant Raman coupling introduces two dressed modes, denoted by $\hat{a}_{j,\pm}=(\hat{b}_{j,1}\pm\hat{b}_{j+1,-1})/\sqrt{2}$ with an energy gap $2\lambda_0$ between them [see Fig. 1(a)]. In the regime $\lambda_0 \simeq q \gg U_0$, only the lower-

energy modes $\hat{a}_{j,-}$ are relevant, since two adjacent ones are resonant to the mode $\hat{b}_{j,0}$ during the spin-exchange process $\sim U_2 \hat{a}_{j-1,-} \hat{b}_{j,0}^{\dagger} \hat{b}_{j,0}^{\dagger} \hat{a}_{j,-}$ (included in the U_2 term of $\hat{H}_{\rm int}$), whereas the higher-energy modes $\hat{a}_{j,+}$ are off-resonance and can thus be ignored.

Now we formally construct the U(1) lattice gauge model. We define the spin-0 mode $\hat{b}_{j,0}$ as the gauge field, schematically denoted by the ovals in Fig. 1(b), and define the lower-lying dressed mode $\hat{a}_{j,-}$ as the matter field, indicated by circles in Fig. 1(b). By restricting that there are at most two particles on a gauge mode and at most one particle on a matter mode, the effective Hamiltonian in terms of matter and gauge fields can be obtained as

$$\hat{H}_{\text{eff}} = -\frac{U_2}{2} \sum_{j} (\hat{a}_{j-1,-} \hat{b}_{j,0}^{\dagger} \hat{b}_{j,0}^{\dagger} \hat{a}_{j,-} + \text{H.c.}) + m \sum_{j} \hat{N}_j + \frac{\tilde{U}}{2} \sum_{j} \hat{N}_{j-1} \hat{N}_j,$$
 (7)

with $m \equiv q - \lambda_0 - U_0/2$ and $\tilde{U} \equiv (U_0 - U_2)/2$. We have defined the number operator of the matter field as $\hat{N}_j = \hat{a}_{j,-}^{\dagger} \hat{a}_{j,-}$. The occupation restriction can be satisfied by a proper preparation of the initial state [37]. $\hat{H}_{\rm eff}$ carries a global translational symmetry and a local U(1) gauge symmetry generated by the local Gauss operator,

$$\hat{G}_j = \hat{N}_j + \frac{\hat{n}_{j+1,0} + \hat{n}_{j,0}}{2} - 1, \tag{8}$$

which is defined on a building block consisting of two neighboring gauge fields and one matter field in the middle, as illustrated in Fig. 1(b). Here we emphasize that the U(1) gauge invariance is valid in the parameter regime $\lambda_0 \simeq q \gg U_0$, out of which the conservation of \hat{G}_j will be broken. This point will be further verified in Appendix A, where a fully numerical calculation is carried out in the context of quench dynamics (see Sec. IV) using the original Hamiltonian Eqs. (4) and (6) with all the modes present. There the effects of $\lambda_0 \simeq q \gg U_0$ on \hat{G}_j will be clearly demonstrated.

To characterize the relation between our effective Hamiltonian \hat{H}_{eff} and the LSM \hat{H}_{LSM} [Eq. (1)], we perform the Jordan-Wigner transformation on the matter fields $\hat{a}_{j,-}$ to map them into fermions. We additionally map gauge fields to spin-1/2 Pauli spins using the relations

$$\hat{\sigma}_{j}^{+} \leftrightarrow \frac{1}{\sqrt{2}} \hat{b}_{j,0}^{\dagger} \hat{b}_{j,0}^{\dagger}, \ \hat{\sigma}_{j}^{-} \leftrightarrow \frac{1}{\sqrt{2}} \hat{b}_{j,0} \hat{b}_{j,0}, \ \hat{\sigma}_{j}^{z} \leftrightarrow \hat{n}_{j,0} - 1.$$
 (9)

A subsequent particle-hole transformation on the odd-site matter fields $\hat{\psi}_{j\in \text{odd}} \to \hat{\psi}_{j\in \text{odd}}^{\dagger}$ and gauge flipping on the odd sites $\hat{\sigma}_{j\in \text{odd}}^{+} \to -\hat{\sigma}_{j\in \text{odd}}^{-}$, $\hat{\sigma}_{j\in \text{odd}}^{z} \to -\hat{\sigma}_{j\in \text{odd}}^{z}$ reform the effective Hamiltonian \hat{H}_{eff} into

$$\begin{split} \hat{H}_{\mathrm{f}} &= -\frac{U_2}{\sqrt{2}} \sum_{j} (\hat{\psi}_{j-1}^{\dagger} \hat{\sigma}_{j}^{+} \hat{\psi}_{j} + \mathrm{H.c.}) \\ &+ \left(\frac{\tilde{U}}{2} + m \right) \sum_{j} (-1)^{j} \hat{\psi}_{j}^{\dagger} \hat{\psi}_{j} - \frac{\tilde{U}}{2} \sum_{j} \hat{\psi}_{j-1}^{\dagger} \hat{\psi}_{j-1} \hat{\psi}_{j}^{\dagger} \hat{\psi}_{j}. \end{split}$$

Following the same manner, Gauss's law in terms of the fermions and the gauge spins is given by

$$\hat{G}_j = \hat{\psi}_j^{\dagger} \hat{\psi}_j - \frac{\hat{\sigma}_{j+1}^z - \hat{\sigma}_j^z}{2} + \frac{1}{2} [(-1)^j - 1], \quad (11)$$

which is conserved, i.e., $[\hat{G}_j, \hat{H}_f] = 0$. By comparing \hat{H}_f with \hat{H}_{LSM} [Eq. (1)] one can observe that, in the case of $\tilde{U} = 0$, \hat{H}_f reproduces the conventional LSM with parameter relations $U_2/\sqrt{2} \leftrightarrow t$ and $\tilde{U}/2 + m \leftrightarrow m$.

The Hamiltonian \hat{H}_f provides the following QED interpretation of the effective Hamiltonian \hat{H}_{eff} . The occupation of even and odd matter sites respectively represent the electrons and the positrons [see Fig. 1(b)], and the spin-exchange interaction $(\sim U_2 \hat{a}_{j-1,-} \hat{b}_{j,0}^{\dagger} \hat{b}_{j,0}^{\dagger} \hat{a}_{j,-})$ describes the process that a pair of electron and positron annihilate each other, generating the photons (gauge bosons). For the current case with gauge fields being spin-1/2 Pauli spins, the photon generation is reflected by the direction inversion of the electric field. Within a building block, the local Gauss operator \hat{G}_i ensures the total flux of the electric field being equal to the number of charged particles, representing the manifestation of Gauss's law. For finite \tilde{U} , $\hat{H}_{\rm f}$ additionally possesses a nearestsite matter-matter interaction $\sim \tilde{U} \hat{\psi}_{i-1}^{\dagger} \hat{\psi}_{j-1} \hat{\psi}_{i}^{\dagger} \hat{\psi}_{j}$, which has no counterpart in the conventional LSM. This term comes from the intrinsic interactions of the spin-1 BEC [Eq. (4)] and will lead to a rich phase diagram as will be shown below.

III. PHASE DIAGRAM

We discuss the equilibrium phases at 1/3 filling, i.e., a total of L particles for a chain with L lattice sites, and focus on the gauge sector with no background charges, i.e., $\{G_j\} = 0$ [16], with G_j being the quantum number of \hat{G}_j . In this case, four occupation configurations, $|0_10\rangle$, $|2_00\rangle$, $|0_02\rangle$, and $|1_01\rangle$, are allowed in a building block, as displayed in Fig. 2(a), where $|n_{j,0N_j}n_{j+1,0}\rangle$ denotes the Fock basis. Since the state $|1_01\rangle$ is a dark state uncoupled to the other three states through the U_2 interaction, we restrict our discussion within the subspace spanned by the remaining three states.

We plot the ground-state phase diagram in the m- U_2 plane in Fig. 2(b) obtained via numerically diagonalizing \hat{H}_{eff} with L=18. A disordered phase D and two ordered phases \mathbb{Z}_2 and \mathbb{Z}_3 are identified. Three phases exhibit different groundstate degeneracy: the disordered phase D is nondegenerate, whereas the ordered phases \mathbb{Z}_2 and \mathbb{Z}_3 possess two- and threefold degeneracy, respectively. In Figs. 2(d1)-2(d3), we show particle number distributions of the three phases and their QED analog at $U_2 = 0$. Clearly, the phase D exhibits a configuration with all the matter fields being occupied whose wave function $|D\rangle = |\cdots 0_1 0_1 0_1 \cdots\rangle$ preserves the translational symmetry of $\hat{H}_{\rm eff}$. On the other hand, the ordered phase \mathbb{Z}_2 (\mathbb{Z}_3) spontaneously breaks the translational symmetry in a \mathbb{Z}_2 (\mathbb{Z}_3) way such that the two (three) ground-state wave functions, $|\mathbb{Z}_2\rangle = |\cdots 2_0 0_0 2_0 \cdots\rangle$ and $|\overline{\mathbb{Z}_2}\rangle = |\cdots 0_0 2_0 0_0 \cdots\rangle$ $(|\mathbb{Z}_3\rangle = |\cdots 2_0 0_1 0_0 \cdots \rangle, |\overline{\mathbb{Z}_3}\rangle = |\cdots 0_0 2_0 0_1 \cdots \rangle \text{ and } |\overline{\mathbb{Z}_3}\rangle =$ $|\cdots 0_1 0_0 2_0 \cdots\rangle$), are energy degenerate. We emphasize that in the conventional LSM with $\tilde{U} = 0$ (i.e., $U_0 = U_2$), only the D and the \mathbb{Z}_2 phases can be found, with phase transition

(10)

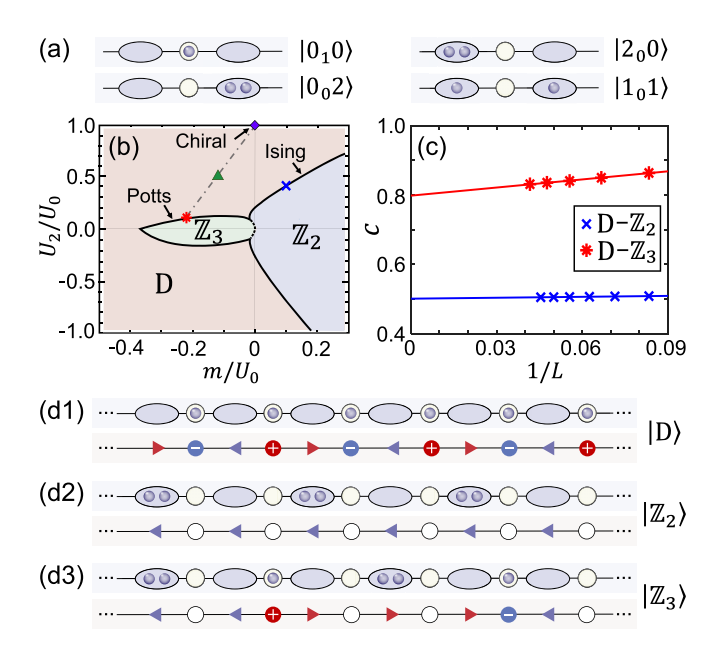


FIG. 2. (a) Four allowed configurations in a building block within the $\{G_j\}=0$ gauge sector. (b) Ground-state phase diagram in the m- U_2 plane, where the dashed and the solid lines respectively denote the first- and second-order phase boundary. In the diagram, the dot-dashed line satisfying $\tilde{U}=-2m$ connects the chiral-symmetric point (diamond) to the Potts critical point (star). On this line we track the $|\mathbb{Z}_3\rangle$ -related quantum scars as discussed in Fig. 3. (c) Finite-size scaling analysis of the central charge c on the second-order phase transitions D- \mathbb{Z}_2 and D- \mathbb{Z}_3 with the cross and the star corresponding to the critical points located at $(m \simeq 0.1U_0, U_2 = 0.4U_0)$ and $(m \simeq -0.22U_0, U_2 = 0.1U_0)$ in (b), respectively. (d) Occupation configurations (upper line) and the corresponding QED analogy (lower line) of the three states $|D\rangle$, $|\mathbb{Z}_2\rangle$, and $|\mathbb{Z}_3\rangle$ at $U_2 = 0$. For $U_2 \neq 0$, populations in individual sites are no longer conserved. However, the ground-state degeneracy in each phase remains the same.

D- \mathbb{Z}_2 being the Coleman's transition [14,16,38]. Therefore the \mathbb{Z}_3 -ordered phase is new and has no counterpart in the conventional LSM. In the phase diagram, the \mathbb{Z}_3 phase exists in the regime with strong matter-field interaction \tilde{U} (i.e., $U_2 \ll U_0$). The existence of the \mathbb{Z}_3 phase stems from the competition between the negative mass m < 0 and $\tilde{U} > 0$: the former favors all the matter fields being occupied, while the latter hinders two neighboring matter fields being occupied simultaneously. From an experimental point of view, the two most commonly used spin-1 species, 23 Na and 87 Rb, both feature a strong \tilde{U} , making the physics predicted in our work quite feasible in practice [27,28].

In the phase diagram, we identify phase transitions between the disordered phase and the ordered phases, $D-\mathbb{Z}_2$ and $D-\mathbb{Z}_3$, to be of second order, while the transition between the two ordered phases $\mathbb{Z}_2-\mathbb{Z}_3$ is of first order. The phase boundaries as well as the transition orders are determined by whether the first- or the second-order derivatives of the ground-state energy with respect to the parameters (m or U_2) exhibit discontinuity or not. Furthermore, the second-order transitions $D-\mathbb{Z}_2$ and $D-\mathbb{Z}_3$ respectively belong to the Ising and the three-state Potts universality classes, whose low-energy critical behaviors are described by the conformal field

theory with different central charges c [39]. Practically, one can extract c through fitting the curve of the von Neumann entropy [40],

$$S(l_A) = \frac{c}{3} \ln \left[\frac{L}{\pi} \sin \left(\frac{\pi l_A}{L} \right) \right] + s', \tag{12}$$

where l_A is the length of subsystem A and s' is a nonuniversal factor. The von Neumann entropy is given by $S(l_A) = -\text{Tr}(\hat{\rho}_A \log \hat{\rho}_A)$, with $\hat{\rho}_A$ being the reduced density matrix. In Fig. 2(c) we show the dependence of c as a function of the chain length L at two critical points [corresponding to the cross and the star in Fig. 2(b)], in which one can observe that the transitions D- \mathbb{Z}_2 and D- \mathbb{Z}_3 exhibit c = 0.5 and c = 0.8 in the thermodynamic limit $1/L \to 0$, clearly indicating the Ising and the three-state Potts universality classes, respectively [39].

IV. QUENCH DYNAMICS AND QUANTUM SCARS

Since we fix the gauge sector ($\{G_j\}=0$), the matter field and the gauge field are no longer independent. Substituting Eq. (9) into the Gauss operator [Eq. (8)], the U(1) lattice gauge model $\hat{H}_{\rm eff}$ can therefore be mapped to a spin-1/2 chain by eliminating the matter fields [20], i.e., $\hat{a}_{j-1,-}\hat{b}_{j,0}^{\dagger}\hat{b}_{j,0}^{\dagger}\hat{a}_{j,-}+$ H.c. $\leftrightarrow \hat{\sigma}_j^x$ and $\hat{N}_j \leftrightarrow -(\hat{\sigma}_j^z+\hat{\sigma}_{j+1}^z)/2$. Following this rule, the mapped spin Hamiltonian takes the form

$$\hat{H}_{s} = -\frac{U_{2}}{\sqrt{2}} \sum_{j} \hat{P}_{j-1} \hat{\sigma}_{j}^{x} \hat{P}_{j+1} - m \sum_{j} \hat{\sigma}_{j}^{z} + \frac{\tilde{U}}{4} \sum_{j} \left(\hat{\sigma}_{j}^{z} \hat{\sigma}_{j+1}^{z} + \frac{1}{2} \hat{\sigma}_{j}^{z} \hat{\sigma}_{j+2}^{z} \right), \tag{13}$$

with $\hat{P}_j = (1 - \hat{\sigma}_j^z)/2$ the projection operator, which projects out the cases of two neighboring spins being polarized up simultaneously. This projection is necessary to make sure that the system remains in the $\{G_i\} = 0$ sector, and the resulting states can be described by the three allowed configurations shown in Fig. 2(a). Particularly at $\tilde{U} = m = 0$ [denoted by the diamond in Fig. 2(b)], \hat{H}_s reproduces the PXP model [41], which was originally realized in a Rydberg chain [19]. The PXP Hamiltonian carries a symmetry $\chi \hat{H}_s \chi = -\hat{H}_s$ with $\chi = \prod_i \hat{\sigma}_i^z$. As a result, the energy spectrum is symmetric about $\epsilon = 0$. This symmetry corresponds to the chiral symmetry of the original lattice gauge model, i.e., $\mathcal{RT}(\hat{H}_f) =$ $-\hat{H}_{\rm f}$, with \mathcal{R} and \mathcal{T} respectively representing the particlehole transformation and the one-site translation. The PXP model is well known to lead to dynamical revivals, which refer to the phenomenon that the postquench evolutions of the Rydberg $|\mathbb{Z}_2\rangle$ and $|\mathbb{Z}_3\rangle$ charge-density waves (CDWs) exhibit periodic recoveries and slow thermalization [19]. This revival can be attributed to the quantum many-body scar states [41–43], which are the low-entropy eigenstates of the PXP Hamiltonian that violate the eigenstate thermalization hypothesis.

The $|\mathbb{Z}_2\rangle$ and $|\mathbb{Z}_3\rangle$ ordered states in our current model correspond exactly to the Rydberg $|\mathbb{Z}_2\rangle$ and $|\mathbb{Z}_3\rangle$ CDW states, and hence our model would also exhibit the dynamical revivals by quenching these two states into the chiral point. We perform such numerics by exactly diagonalizing (ED) the effective

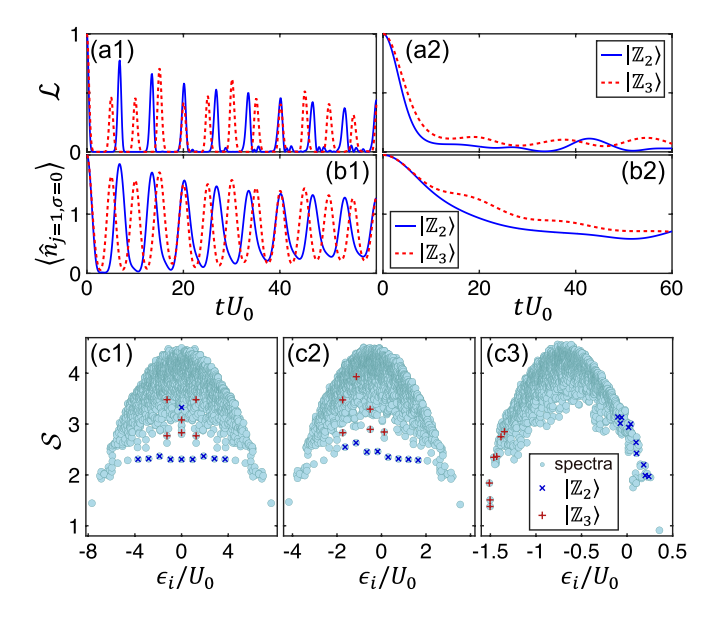


FIG. 3. Dynamics of the Loschmidt echo \mathcal{L} (a) and occupation on the first gauge site (b) as $|\mathbb{Z}_2\rangle$ and $|\mathbb{Z}_3\rangle$ states are quenched to the chiral-symmetric point (a1, b1) and the Potts critical point (a2, b2). (c) The von Neumann entropy \mathcal{S} plotted vs energy spectra ϵ_i at the chiral [denoted by diamond in Fig. 2(b)], the middle (triangle), and the Potts critical (star) points on the line of $\tilde{U}=-2m$ in (c1)–(c3), where crosses and plus signs indicate the scar states with large overlap to the $|\mathbb{Z}_2\rangle$ and $|\mathbb{Z}_3\rangle$ states, respectively. In the calculation, we take L=18, and \mathcal{S} is calculated using $l_A=L/2$.

Hamiltonian \hat{H}_{eff} and plot the evolution of the Loschmidt echo $\mathcal{L}(t) = |\langle \psi(0) | \psi(t) \rangle|^2$ and the occupation $\langle \hat{n}_{j,\sigma=0}(t) \rangle$ on one gauge site in Figs. 3(a1) and 3(b1). $|\psi(0)\rangle$ is initialized by $|\mathbb{Z}_2\rangle$ (solid line) and $|\mathbb{Z}_3\rangle$ (dashed line) states, respectively. The periodic oscillating curves clearly demonstrate the dynamical revivals. In Fig. 3(c1) we show the eigenspectrum ϵ_i with vertical axis S denoting the bipartite von Neumann entropy of eigenstates $|\epsilon_i\rangle$, where the scar states responsible for the $|\mathbb{Z}_2\rangle$ and $|\mathbb{Z}_3\rangle$ revivals are marked by cross and plus signs, respectively. These scars are selected according to the projective probability $|\langle \epsilon_i | \mathbb{Z}_2 \rangle|^2$ and $|\langle \epsilon_i | \mathbb{Z}_3 \rangle|^2$ above the threshold ≥ 0.03 . As one can see, the scar states possess equal energy intervals and relatively low entropy within the spectrum. The energy interval $\Delta \epsilon$ matches well with the revival period T of $\mathcal{L}(t)$ via the relation $T = 2\pi/\Delta\epsilon$. In comparison, the dynamics of the same quantities, quenched to the Potts critical point, are plotted in Figs. 3(a2) and 3(b2), where the physical quantities exhibit fast quantum thermalization without oscillation. To check the validity of these results, in Appendix A we also carry out numerical calculations based on the original Hamiltonian Eqs. (4) and (6) using the technique called the time evolution of matrix product states (tMPS) [44]. The tMPS results are in excellent agreement with the ED results when the condition $\lambda_0 \simeq q \gg U_0$ is satisfied. This also serves as a confirmation of the validity of the effective Hamiltonian \hat{H}_{eff} .

The origin of the scars is of tremendous interest. Recently, Yao and co-workers observed that the $|\mathbb{Z}_2\rangle$ -related quantum scars migrate from the low-energy low-entropy states of the Ising transition [45]. Considering the diagram Fig. 2(b) pos-

sesses a Potts criticality, hence now we have an opportunity in tracing the origin of the scar states associated with the $|\mathbb{Z}_3\rangle$ dynamics. We focus on the line $\tilde{U}=-2m$ [see the dot-dashed line in diagram Fig. 2(b)] and show the $|\mathbb{Z}_2\rangle$ - as well as the $|\mathbb{Z}_3\rangle$ -related scar spectra at the chiral-symmetric (diamond), middle (triangle), and Potts critical (star) points in Figs. 3(c1)–3(c3), respectively. One may immediately observe that the spectra 3(c2) and 3(c3) are asymmetric about $\epsilon=0$ due to the chiral symmetry breaking induced by the finite \tilde{U} interaction. Furthermore, as the Potts critical point is approached, $|\mathbb{Z}_3\rangle$ -and $|\mathbb{Z}_2\rangle$ -related scars respectively transfer to the low- and high-energy regimes, indicating that the scars associated with $|\mathbb{Z}_3\rangle$ originate from the low-energy low-entropy states of the Potts transition.

V. SUMMARY AND OUTLOOK

We propose a scheme to synthesize the U(1) gauge invariance in a spin-1 Bose gas. Unlike in previous realizations [14,15], the interactions in the spinor gas naturally leads a matter-field interaction term in the effective U(1) gauge model, which gives rise to a new \mathbb{Z}_3 -ordered phase. This ordered phase connects to the disordered phase by the Potts criticality, whose low-energy eigenstates are found to be the origin of quantum scar states responsible for the anomalous dynamical revivals of the $|\mathbb{Z}_3\rangle$ states. There are several follow-up questions. In the context of high-energy physics, the continuous deconfined Schwinger model is known to be equivalent to the sine-Gordon model under bosonization [16]. The matter-field interaction seems to only modify the free part. In this picture, clarification of the physical mechanism of the \mathbb{Z}_3 -ordered phase would require a more detailed calculation in the future. In the context of quantum thermodynamics, why do the ordered states, $|\mathbb{Z}_2\rangle$ and $|\mathbb{Z}_3\rangle$, tend to be thermalized at quantum criticality? Can the matter-field interaction induce many-body localization dynamics [46,47] as different gauge sectors are involved? Very recently, we notice that two works [48,49] have explored the possibility of tuning the topological angle in the synthetic LSM. It will be also interesting to study the combined effect of topological angle and the matter-field interaction.

ACKNOWLEDGMENTS

L.C. would like to thank Shang Liu, Yanting Cheng, Xin Chen, and Zhiyuan Yao for the insightful discussion. L.C. acknowledges support from the NSF of China (Grants No. 12174236 and No. 12147215); H.P. acknowledges support from the US NSF and the Welch Foundation (Grant No. C-1669).

APPENDIX: QUENCH DYNAMICS USING TMPS

In the derivation of the effective Hamiltonian $\hat{H}_{\rm eff}$ [Eq. (7)], we focus on the parameter regime $\lambda_0 \simeq q \gg U_0$ in which the off-resonant $\hat{a}_{j,+}$ modes can be neglected. Therefore the parameter condition $\lambda_0 \simeq q \gg U_0$ stands as the prerequisite for our effective Hamiltonian $\hat{H}_{\rm eff}$ and the U(1) gauge invariance. Here, let us in detail discuss how this condition would affect our lattice gauge model in the context of quench

dynamics. To this end, we adopt the tMPS method, which is a powerful tool for the large-scale simulation of one-dimensional quantum systems out of equilibrium [44]. Our numerical simulation is based on the original Hamiltonian Eqs. (4) and (6) with all the modes present. We set the lattice length L=54 and quench the $|\mathbb{Z}_2\rangle=|\cdots 2_00_02_0\cdots\rangle$ and $|\mathbb{Z}_3\rangle=|\cdots 2_00_10_0\cdots\rangle$ states to the chiral point $\tilde{U}=m=0$. We examine two operators that are experimentally measurable: one is the particle number of a single gauge site, e.g., $\langle \hat{n}_{j,\sigma=0} \rangle$, and the other is the averaged expectation of the Gauss operator, i.e.,

$$\bar{G} = \frac{1}{L} \sum_{i} |\langle \hat{G}_{j} \rangle|, \tag{A1}$$

where $\langle \hat{G}_j \rangle$, according to the definition [Eq. (8)], is simply the measurement on the local particle numbers within a building block. In the $\{G_j\}=0$ gauge sector, since \hat{G}_j is conserved, the deviation of \bar{G} from zero reflects the breaking of the gauge invariance.

In Figs. 4(a) and 4(b) we show the dynamics of these two observables with respect to the $|\mathbb{Z}_2\rangle$ initial state [(a1) and (b1)] and the $|\mathbb{Z}_3\rangle$ initial state [(a2) and (b2)]. In each subfigure, the dot-dashed, dashed, and dotted lines indicate the cases with $U_0/\lambda_0 = 1$, $U_0/\lambda_0 = 0.1$, and $U_0/\lambda_0 = 0.01$, corresponding to the situations that the condition $\lambda_0 \simeq q \gg U_0$ is unsatisfied, just satisfied, and strictly satisfied, respectively. In comparison, the dynamics of $\langle \hat{n}_{j,\sigma=0} \rangle$ obtained by exactly diagonalizing the effective Hamiltonian \hat{H}_{eff} are also plotted by solid lines in Figs. 4(a1) and 4(a2). One can clearly observe that, for the latter two cases $(U_0/\lambda_0 = 0.1 \text{ and } U_0/\lambda_0 = 0.01)$, the tMPS dynamics of $\langle \hat{n}_{1,0} \rangle$ are in good agreement with those obtained by the ED method, and \bar{G} exhibits small oscillation around zero. In contrast, for the case of $U_0/\lambda_0 = 1$, the resulting $\langle \hat{n}_{1,0} \rangle$ exhibits a large discrepancy to the ED's results, accompanied by the large deviation of the local conservation

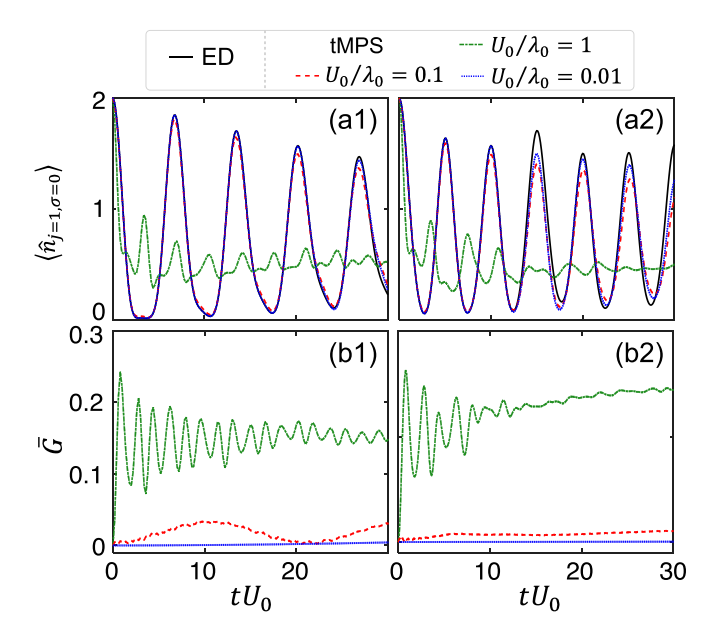


FIG. 4. Upper row: Dynamical evolution of the particle number of the first gauge site $\langle \hat{n}_{j=1,\sigma=0} \rangle$ under the government of the chiral-symmetric Hamiltonian with $\tilde{U}=m=0$, where (a1) and (a2) correspond to the cases with initial states being $|\mathbb{Z}_2\rangle$ and $|\mathbb{Z}_3\rangle$, respectively. Bottom row: Evolution of the averaged expectation of the Gauss operator \tilde{G} [Eq. (A1)] with initial states being $|\mathbb{Z}_2\rangle$ (b1) and $|\mathbb{Z}_3\rangle$ (b2). In each subfigure, the solid line denotes the ED's result based on the effective Hamiltonian $\hat{H}_{\rm eff}$ in the gauge sector $\{G_j\}=0$; the dot-dashed, dashed, and dotted lines respectively correspond to the cases $U_0/\lambda_0=1,0.1,0.01$, indicating the results obtained by the tMPS method using the original Hamiltonian Eqs. (4) and (6). In our calculation, we fix L=54 and L=18 for the tMPS and ED simulations, respectively.

 \bar{G} from zero. These results serve as a criterion for the validity of our effective model $\hat{H}_{\rm eff}$.

^[1] S. Weinberg, *The Quantum Theory of Fields* (Cambridge University Press, Cambridge, New York, 1995).

^[2] R. P. Feynman, *QED: The Strange Theory of Light and Matter* (Princeton University Press, Princeton, NJ, 2006).

^[3] W. Marciano and H. Pagels, Quantum chromodynamics, Phys. Rep. 36, 137 (1978).

^[4] J. B. Kogut, The lattice gauge theory approach to quantum chromodynamics, Rev. Mod. Phys. **55**, 775 (1983).

^[5] H. Meyer-Ortmanns, Phase transitions in quantum chromodynamics, Rev. Mod. Phys. **68**, 473 (1996).

^[6] N. Goldman, G. Juzeliūnas, P. Öhberg, and I. B. Spielman, Light-induced gauge fields for ultracold atoms, Rep. Prog. Phys. 77, 126401 (2014).

^[7] Y.-J. Lin, R. L. Compton, K. Jiménez-García, W. D. Phillips, J. V. Porto, and I. B. Spielman, A synthetic electric force acting on neutral atoms, Nat. Phys. 7, 531 (2011).

^[8] Y.-J. Lin, R. L. Compton, K. Jiménez-García, J. V. Porto, and I. B. Spielman, Synthetic magnetic fields for ultracold neutral atoms, Nature (London) 462, 628 (2009).

^[9] Y.-J. Lin, K. Jiménez-García, and I. B. Spielman, Spin-orbitcoupled Bose-Einstein condensates, Nature (London) 471, 83 (2011).

^[10] P. Wang, Z.-Q. Yu, Z. Fu, J. Miao, L. Huang, S. Chai, H. Zhai, and J. Zhang, Spin-Orbit Coupled Degenerate Fermi Gases, Phys. Rev. Lett. 109, 095301 (2012).

^[11] L. W. Cheuk, A. T. Sommer, Z. Hadzibabic, T. Yefsah, W. S. Bakr, and M. W. Zwierlein, Spin-Injection Spectroscopy of a Spin-Orbit Coupled Fermi Gas, Phys. Rev. Lett. 109, 095302 (2012).

^[12] F. Görg, K. Sandholzer, J. Minguzzi, R. Desbuquois, M. Messer and T. Esslinger, Realization of density-dependent Peierls phases to engineer quantized gauge fields coupled to ultracold matter, Nat. Phys. 15, 11661 (2019).

^[13] L. W. Clark, B. M. Anderson, L. Feng, A. Gaj, K. Levin, and C. Chin, Observation of Density-Dependent Gauge Fields in a Bose-Einstein Condensate Based on Micromotion Control in a Shaken Two-Dimensional Lattice, Phys. Rev. Lett. 121, 030402 (2018).

- [14] B. Yang, H. Sun, R. Ott, H.-Y. Wang, T. V. Zache, J. C. Halimeh, Z.-S. Yuan, P. Hauke, and J.-W. Pan, Observation of gauge invariance in a 71-site Bose-Hubbard quantum simulator, Nature (London) 587, 392 (2020).
- [15] A. Mil, T. V. Zache, A. Hegde, A. Xia, R. P. Bhatt, M. K. Oberthaler, P. Hauke, J. Berges, and F. Jendrzejewski, A Scalable realization of local U(1) gauge invariance in cold atomic mixtures, Science 367, 1128 (2020).
- [16] S. R. Coleman, More about the massive Schwinger model, Ann. Phys. (NY) 101, 239 (1976).
- [17] D. Banerjee, M. Dalmonte, M. Müller, E. Rico, P. Stebler, U.-J. Wiese, and P. Zoller, Atomic Quantum Simulation of Dynamical Gauge Fields Coupled to Fermionic Matter: From String Breaking to Evolution after a Quench, Phys. Rev. Lett. 109, 175302 (2012).
- [18] T. Pichler, M. Dalmonte, E. Rico, P. Zoller, and S. Montangero, Real-Time Dynamics in U(1) Lattice Gauge Theories with Tensor Networks, Phys. Rev. X 6, 011023 (2016).
- [19] H. Bernien, S. Schwartz, A. Keesling, H. Levine, A. Omran, H. Pichler, S. Choi, A. S. Zibrov, M. Endres, M. Greiner, V. Vuletić, and M. D. Lukin, Probing many-body dynamics on a 51-atom quantum simulator, Nature (London) 551, 579 (2017).
- [20] F. M. Surace, P. P. Mazza, G. Giudici, A. Lerose, A. Gambassi, and M. Dalmonte, Lattice Gauge Theories and String Dynamics in Rydberg Atom Quantum Simulators, Phys. Rev. X 10, 021041 (2020).
- [21] T. M. R. Byrnes, P. Sriganesh, R. J. Bursill, and C. J. Hamer, Density matrix renormalization group approach to the massive Schwinger model, Phys. Rev. D 66, 013002 (2002).
- [22] S. Thompson and G. Siopsis, Quantum computation of phase transition in the massive Schwinger model, Quantum Sci. Technol. 7, 035001 (2022).
- [23] M. E. Peskin, An Introduction to Quantum Field Theory (CRC Press, Boca Raton, FL, 1995).
- [24] R. D. Pisarski, A. M. Tsvelik, and S. Valgushev, How transverse thermal fluctuations disorder a condensate of chiral spirals into a quantum spin liquid, Phys. Rev. D 102, 016015 (2020).
- [25] D. J. Gross and A. Neveu, Dynamical symmetry breaking in asymptotically free field theories, Phys. Rev. D 10, 3235 (1974).
- [26] W. E. Thirring, A soluble relativistic field theory, Ann. Phys. 3, 91 (1958).
- [27] Y. Kawaguchi and M. Ueda, Spinor Bose-Einstein condensates, Phys. Rep. **520**, 253 (2012).
- [28] D. M. Stamper-Kurn and M. Ueda, Spinor Bose gases: Symmetries, magnetism, and quantum dynamics, Rev. Mod. Phys. **85**, 1191 (2013).
- [29] S. Chandrasekharan and U.-J. Wiese, Quantum link models: A discrete approach to gauge theories, Nucl. Phys. B 492, 455 (1997).
- [30] B. Oruç and A. Keskinsezer, Structural setting of the northeastern BiGa peninsula (Turkey) from tilt derivatives of gravity gradient tensors and magnitude of horizontal gravity components, Pure Appl. Geophys. 165, 1913 (2008).
- [31] R. Omori, T. Kobayashi, and A. Suzuki, Observation of a single-beam gradient-force optical trap for dielectric particles in air, Opt. Lett. **22**, 816 (1997).

- [32] H. Miyake, G. A. Siviloglou, C. J. Kennedy, W. C. Burton, and W. Ketterle, Realizing the Harper Hamiltonian with Laser-Assisted Tunneling in Optical Lattices, Phys. Rev. Lett. 111, 185302 (2013).
- [33] T.-L. Ho, Spionor Bose Condensates in Optical Traps, Phys. Rev. Lett. **81**, 742 (1998).
- [34] T. Ohmi and K. Machida, Bose-Einstein condensation with internal degrees of freedom in alkali atoms gases, J. Phys. Soc. Jpn. 67, 1822 (1998).
- [35] X.-J. Liu, K. T. Law, and T. K. Ng, Realization of 2D Spin-Orbit Interaction and Exotic Topological Orders in Cold Atoms, Phys. Rev. Lett. 112, 086401 (2014).
- [36] Z. Wu, L. Zhang, W. Sun, X.-T. Xu, B.-Z. Wang, S.-C. Ji, Y. Deng, S. Chen, X.-J. Liu, and J.-W. Pan, Realization of two-dimensional spin-orbit coupling for Bose-Einstein condensates, Science 354, 83 (2016).
- [37] B. Yang, H. Sun, C.-J. Huang, H.-Y. Wang, Y. Deng, H.-N. Dai, Z.-S. Yuan, J.-W. Pan, Cooling and entangling ultracold atoms in optical lattices, Science 369, 550 (2020).
- [38] E. Rico, T. Pichler, M. Dalmonte, P. Zoller, and S. Montangero, Tensor Networks for Lattice Gauge Theories and Atomic Quantum Simulation, Phys. Rev. Lett. 112, 201601 (2014).
- [39] P. Di Francesco, P. Mathieu, and D. Sénéchal, *Conformal Field Theory* (Springer, New York, 1997).
- [40] P. Calabrese and J. Cardy, Entanglement entropy and quantum field theory, J. Stat. Mech.: Theor. Exp. 0406 P06002 (2004)
- [41] C. J. Turner, A. A. Michailidis, D. A. Abanin, M. Serbyn, and Z. Papić, Quantum scarred eigenstates in a Rydberg atom chain: Entanglement, breakdown of thermalization, and stability to perturbations, Phys. Rev. B 98, 155134 (2018).
- [42] C. J. Turner, A. A. Michailidis, D. A. Abanin, M. Serbyn, and Z. Papić, Weak ergodicity breaking from quantum many-body scars, Nat. Phys. 14, 745 (2018).
- [43] M. Serbyn, D. A. Abanin, and Z. Papić, Quantum many-body scars and weak breaking of ergodicity, Nat. Phys. 17, 675 (2021).
- [44] U. Schollwöck, The density-matrix renormalization group in the age of matrix product states, Ann. Phys. **326**, 96 (2011)
- [45] Z. Yao, L. Pan, S. Liu, and H. Zhai, Quantum many-body scars and quantum criticality, Phys. Rev. B **105**, 125123 (2022).
- [46] D. A. Abanin, E. Altman, I. Bloch, and M. Serbyn, Colloquium: Many-body localization, thermalization, and entanglement, Rev. Mod. Phys. 91, 021001 (2019).
- [47] M. Schreiber, S. S. Hodgman, P. Bordia, H. P. Lüschen, M. H. Fischer, R. Vosk, E. Altman, U. Schneider, and I. Bloch, Observation of many-body localization of interacting fermions in a quasirandom optical lattice, Science **349**, 842 (2015).
- [48] J. C. Halimeh, I. P. McCulloch, B. Yang, and P. Hauke, Tuning the topological θ -angle in cold-atom quantum simulators of gauge theories, arXiv:2204.06570.
- [49] Y. Cheng, S. Liu, W. Zheng, P. Zhang, and H. Zhai, Tunable confinement-deconfinement transition in an ultracold atom quantum simulator, arXiv:2204.06586.